

www.acsabm.org Article

# Role of Microfiltration Membrane Morphology on Nanoparticle Purification to Enhance Downstream Purification of Viral Vectors

Mara Leach, Catherine Cox, Sumith Ranil Wickramasinghe, Malgorzata Chwatko,\* and Dibakar Bhattacharyya\*



Cite This: ACS Appl. Bio Mater. 2024, 7, 3932-3941



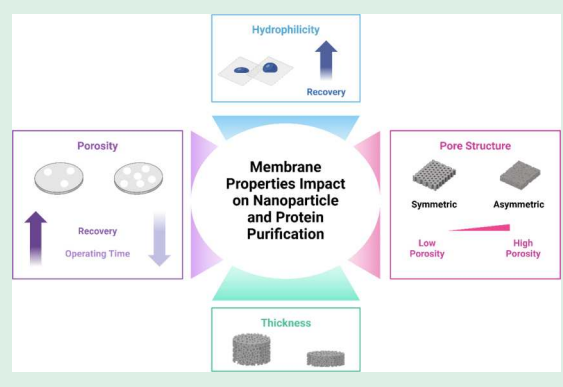
**ACCESS** I

III Metrics & More

Article Recommendations

s Supporting Information

ABSTRACT: In the rapidly advancing realms of gene therapy and biotechnology, the efficient purification of viral vectors is pivotal for ensuring the safety and efficacy of gene therapies. This study focuses on optimizing membrane selection for viral vector purification by evaluating key properties, including porosity, thickness, pore structure, and hydrophilicity. Notably, we employed adeno-associated virus (AAV)-sized nanoparticles (20 nm), 200 nm particles, and bovine serum albumin (BSA) to model viral vector harvesting. Experimental data from constant pressure normal flow filtration (NFF) at 1 and 2 bar using four commercial flat sheet membranes revealed distinct fouling behaviors. Symmetric membranes predominantly showed internal and external pore blockage, while asymmetric membranes formed a cake layer on the surface. Hydrophilicity exhibited a positive correlation with recovery, demonstrating



an enhanced recovery with increased hydrophilicity. Membranes with higher porosity and interpore connectivity showcased superior throughput, reduced operating time, and increased recovery. Asymmetric polyether sulfone (PES) membranes emerged as the optimal choice, achieving ~100% recovery of AAV-sized particles, an ~44% reduction in model cell debris (200 nm particles), an ~35% decrease in BSA, and the fastest operating time of all membranes tested. This systematic investigation into fouling behaviors and membrane properties not only informs optimal conditions for viral vector recovery but also lays the groundwork for advancing membrane-based strategies in bioprocessing.

KEYWORDS: microfiltration, gene therapy, nanoparticles, viral vectors, bioseparations

# 1. INTRODUCTION

The development of adeno-associated virus serotype 2 (AAV2) as a gene therapy vector has opened new possibilities for the treatment of a wide range of genetic disorders.<sup>1,2</sup> These engineered vectors mimic the behavior of their wild-type counterparts, penetrating host cells and delivering therapeutics. However, despite their promise, the efficient purification of AAV2 vectors remains a complex and resource-intensive process, plagued by multiple challenges at various stages of purification. These challenges arise from the viruses requiring cells to replicate, resulting in a complex mixture of cells, cell debris, organelles, proteins, genetic material, salts, and viruses to purify.<sup>3</sup> At the beginning of the purification process, the harvesting step involves disrupting host cells to release the AAV2 vectors and their associated cellular constituents. Cellular contaminants at this stage can lead to downstream fouling issues, shorter lifespan of chromatographic resins, reduced vector yields, and increased production costs.<sup>1,4</sup>

Conventional methods for the harvest purification step primarily rely on size- and density-based separation techniques, namely, ultracentrifugation, chromatography, and filtration. Ultracentrifugation leverages centrifugal force to segregate components based on differences in density. In this method, a suspension containing a small quantity of viral vector stock solution is combined with cesium chloride (CsCl), iodixanol, or sucrose to isolate the viral vectors from contaminants like cell debris, host cell proteins, DNA, and aggregates.<sup>3,5</sup> However, this purification approach encounters numerous challenges. These include constraints related to scalability, extent of particle recovery, time-intensive procedures, the risk of inducing shear stress on the vectors, and inadequate removal of impurities.<sup>3</sup> Moreover, the need to separate the introduced CsCl, iodixanol, or sucrose solution represents an additional operational step. Chromatography methods are typically reserved for the further downstream steps; however, size exclusion chromatography has been utilized for harvesting.<sup>6</sup> Chromatographic methods are less suited for this application

Received: February 26, 2024
Revised: May 22, 2024
Accepted: May 23, 2024
Published: June 1, 2024





given the larger size of virus particles compared to that of therapeutic proteins. Diffusional limitations lead to prolonged operating times, as well as the need for substantial volumes of salt/buffer solutions for elution, resulting in increased operating costs. These limitations underscore the importance of exploring alternative purification methods, such as membrane filtration, particularly in the context of large-scale viral vector production, where efficiency, cost-effectiveness, and product integrity are paramount.

Depth filtration and tangential flow filtration (TFF) are two widely employed methods for the purification of viral vectors, crucial for various biopharmaceutical applications. Depth filtration operates by trapping particles within the matrix of a porous material, effectively separating impurities from the target viral vectors based on size and density differences. This method is commonly utilized in the initial stages of purification to remove large particulate matter and cell debris, providing a clarified solution for subsequent processing steps. §4,4,7,8 While effective for initial clarification steps, depth filtration may have limited selectivity and can suffer from pore blockage or fouling. 9-11 On the other hand, TFF employs a membranebased separation technique where the feed solution flows tangentially across a membrane, allowing smaller molecules such as viral vectors to pass through while retaining larger impurities.<sup>8,9,11-19</sup> TFF offers precise control over the separation process, enabling the concentration and diafiltration of viral vectors to achieve the desired purity levels. For example, studies conducted by Negrete et al. utilizing polypropylene hollow fiber membranes have demonstrated their ability to achieve efficient separation of particles and proteins, coupled with a negligible cell debris index, thus minimizing damage to viral vector-like particles.<sup>20</sup> This success is mirrored in the work of Besnard et al., who achieved high product recovery rates (>85%) and a 10-fold reduction in operating time by implementing crude harvest clarification membrane trains for viral vector purification. <sup>4</sup> These findings collectively underscore the transformative role of membranes in advancing viral vector purification, offering enhanced efficiency and specificity compared with traditional methods.

Membranes have demonstrated success not only in viral vector purification but also in various other bioprocessing applications. For well established protein purification, e.g., mAbs, membranes play a highly important role in achieving viral clearance. Here the aim is to validate the removal of contaminating virus particles while purifying the protein product. Membrane-based filtration processes effectively remove viruses from protein solutions, ensuring the production of safe and high-quality biotherapeutics. 21,22 Moreover, membranes are integral to viral vector concentration through diafiltration processes. By selectively allowing the passage of water and small solutes while retaining viral vectors, these membranes enable the concentration of viral vectors, enhancing the overall efficiency of downstream processing.<sup>2</sup> The versatility of membranes in different bioprocessing applications underscores their significance in ensuring the safety, purity, and high yield of biotherapeutic products. This success in diverse applications further highlights the potential for membrane-based strategies for viral vector purification.

Synthetic nanoparticles have been increasingly utilized as model particles in process optimization studies.<sup>23–27</sup> This approach enables researchers to investigate and optimize various parameters, such as buffer and surfactant concentrations, for enhanced viral vector-like nanoparticle through-

put.<sup>28</sup> Several investigators have considered the use of model particles as contaminants in water treatment applications.<sup>29,30</sup> In earlier work, done by Chu et al., the retention of 30 nm polystyrene nanoparticle suspensions was investigated as a model for AAV3.<sup>28</sup> Moreover, a recent study investigating single pass tangential flow filtration of 100 nm nanoparticles indicated they are a good model for lentivirus.<sup>23</sup> Overall, the use of nanoparticles provides a controlled and reproducible model, facilitating insights into the dynamics of the purification process, specifically when employing size-based exclusion principles.

Despite the promising advancements, fouling remains a critical challenge, hindering the broader adoption of membranes in bioseparations. Various studies have delved into fouling behavior, revealing the complexities associated with membrane fouling during filtration. <sup>8,14,26,31–40</sup> Understanding and mitigating fouling are essential for optimizing membrane performance and sustaining efficient viral vector harvesting and clarification processes.

However, a notable gap in the current literature pertains to the limited knowledge regarding how membrane characteristics and microstructure impact recovery and operating time during viral vector purification. This critical aspect warrants further investigation to unlock the full potential of membranes in bioprocessing applications. Bridging this gap in understanding will pave the way for tailored membrane designs and operational strategies, ensuring enhanced performance and wider applicability of membranes in viral vector purification processes.

In this study, we systematically investigated commercial membrane characteristics for viral vector purification. The over-reaching goal was to optimize membrane selection for high viral vector particle recovery in short processing time and to understand fouling behavior due to both cell debris and vector particles. Four membranes were evaluated from two different manufactures. A range of membrane materials were tested: polycarbonate (PC), poly(ether sulfone) (PES), and polyvinylidene fluoride (PVDF). Besides being fabricated from different polymers, these four membranes represented a range of membrane properties such as thickness, porosity, hydrophilicity, and pore structure. Constant pressure normal flow filtration (NFF), which allowed for a controlled and efficient platform for assessing the impact of membrane properties, was conducted at operating pressures of 1 and 2 bar. In order to evaluate fouling behavior, the experimental flux values were compared to classical membrane fouling models based on cake layer formation and standard blocking.<sup>41</sup> These results will help guide the design of microfiltration membranes for viral vector purification.

#### 2. MATERIALS AND METHODS

**2.1. Materials.** All experiments were performed using commercially available hydrophilic microfiltration membranes: Durapore, Isopore, and Millipore Express PLUS membranes were provided by MilliporeSigma (Bedford, MA) while hydrophilized PVDF400 was provided by Solecta Membranes (Oceanside, CA).

Fluorescently labeled silica nanoparticles (SUPSIL FLUORO-LINK) were obtained from Superior Silica (Phoenix, AZ) in deionized water. Two different nanoparticles were examined: green 20 nm particles (Ex/Em 495 nm/520 nm) as a model for AAV and red 200 nm particles (Ex/Em 570 nm/595 nm) as a model for small cell debris and aggregates.

RICCA Type I/II water, sodium dodecyl sulfate (SDS) (>98.5%), Tris Buffer plus saline (150 mM NaCl), and bovine serum albumin (BSA) (>98%) were obtained from VWR.

**2.2.** Microfiltration Membranes Characterization. 2.2.1. Hydrophilicity. The hydrophilicity of the membranes was determined by utilizing contact angle measurements (KRÜSS drop shape analyzer). These data were obtained in triplicate by cutting a small sample of the membrane and placing the sample on a glass plate by using double-sided tape. The sample was placed in the KRÜSS drop shape analyzer to measure the contact angle. A small drop of water ( $\sim$ 3  $\mu$ L) was placed on the surface of the membrane, and the angle the droplet made with the surface of the membrane measures the contact angle. Data were obtained for contact angle immediately after dropping the water on the surface and over a period of time. These results are highlighted in S-6.

2.2.2. Porosity. The porosity of the membranes was found using a Micromeritics AccuPyc 1330 gas pycnometer. Clean, dry membrane samples were cut into small circles (1.25 cm radius) in triplicate. The membrane samples were placed in the 10 cm³ cup cylinder and placed in the pycnometer. The pycnometer then was initialized, and helium gas flooded the system, which filled the entire chamber, including the pores of the membrane. The porosity of the membrane was calculated using the equation below.

$$porosity = 1 - \frac{volume_{pycnometer}}{volume_{based on geometry}}$$

Porosity results are highlighted in S-5.

**2.3.** Nanoparticle Suspension. 2.3.1. Preparation. 2.3.1.1. Model Viral Vector. Green, fluorescent 20 nm silica nanoparticles were suspended in RICCA Type I/II water at a concentration of approximately 10<sup>14</sup> particles/mL which represents a typical concentration of AAV viral vector supernatant. 2 0.01% of SDS from Sigma-Aldrich (St. Louis, Missouri) was added to decrease agglomeration and aggregation within the suspension.

2.3.1.2. Model Mixture. Green, fluorescent 20 nm silica nanoparticles were suspended in RICCA Type I/II water at a concentration of approximately 10<sup>14</sup> particles/mL. 200 nm red fluorescent silica particles (200 nm) were suspended in Type I/II water (RICCA) at a concentration of approximately 10<sup>10</sup> particles/mL. Bovine serum albumin (BSA) from VWR at a concentration of approximately 6 mg/mL was added to the mixture suspension (20 and 200 nm) to represent host cell proteins typically seen in bioreactor harvest suspensions. 0.01% of SDS from Sigma-Aldrich (St. Louis, Missouri) was added to decrease agglomeration and aggregation within the suspension.

2.3.1.3. Buffer Effect Suspension. Tris buffer plus saline from VWR was diluted from 20x concentration to 1x concentration (150 mM NaCl) using RICCA Type I/II water. A suspension of green, fluorescent 20 nm silica at a concentration of approximately 10<sup>14</sup> particles/mL was prepared. A suspension of red fluorescent 200 nm silica particles at a concentration of approximately 10<sup>10</sup> particles/mL was also prepared. BSA was added to the suspension at a concentration of approximately 6 mg/mL. 0.01% of SDS (0.01%) was added to decrease agglomeration and aggregation within the suspension.

2.3.2. Characterization. 2.3.2.1. Particle Size and Zeta Potential. The particle size distribution and zeta potential were evaluated by using an Anton Paar particle analyzer. The particle size was determined based on the Stokes—Einstein equation. Particle stability was determined by continually analyzing the suspension every 10 min for 40 min without any additional sonication or mixing. The zeta potential was determined by measuring the electrophoretic mobility of the particles. All results were evaluated in triplicate. These results are highlighted in S-4.

2.3.2.2. Fluorescent Intensity. Fluorescent intensity measurements were performed in triplicate using a 96-well black clear-bottomed plate placed in a BioTeck Synergy hybrid microplate reader. All samples were diluted to a one-part suspension of three parts water prior to placing in microplate reader to unsure that the intensity was

not misrepresented by decreased sensitivity of the microplate reader at high concentrations. All samples were tested in triplicate. The fluorescence intensity was highly linear over the full range of particle concentrations with  $R^2 > 0.98$  highlighted in S-2.

2.3.2.3. BSA Absorbance. BSA concentrations were determined using absorbance measurements at a wavelength of 280 nm. Measurements were performed in triplicate using a 96-well acrylic clear well plate placed in a BioTeck Synergy hybrid microplate reader. All samples were tested in triplicate. The absorbance measurements were highly linear over the full range of particle concentrations, with  $R^2 > 0.99$  highlighted in S-3.

2.4. Scanning Electron Microscopy (SEM) and Electron Diffraction X-ray (EDX) Preparation. Membranes were prepared by completely drying the membrane samples pre- and post filtration. This was done by allowing the membranes to sit for at least overnight under ambient conditions. Once completely dried, the samples were cut into small samples (~1 cm by 1 cm) and placed on the Helios NanoLab 660 SEM insertion disk utilizing conductive double side tape. The borders of the samples were painted with conductive paint (colloidal graphite) to verify stability in the equipment. Finally, all samples were sputter coated by using a sputter coater to prevent charging from the membrane material. They were coated with approximately 3 nm of platinum.

Cross sectional images were prepared by utilizing a freeze-breaking method. The membrane samples were first cut into small rectangular sections ( $\sim$ 1 cm -4 cm) and dipped into liquid nitrogen for at least 30 s or until brittle. The samples were then broken in half and placed on a 90° SEM disk using conductive double-sided tape. The border of the samples were painted with conductive paint (colloidal graphite) to verify stability in the equipment. Finally, all samples were sputter coated using a sputter coater to prevent charging from the membrane material. They were coated with  $\sim$ 3 nm of platinum.

**2.5. Membrane Filtration.** Filtration experiments were completed by using the four membranes outlined in Section 2.2. Membranes were cut into 40 cm² circles that were placed in a normal flow filtration (NFF) glass stirred cell unit from Millipore Sigma. The pressure was adjusted to the desired pressure for each run (1 or 2 bar), and the membranes were then flushed and compacted with 100 mL of Type I/II water through the filtration unit to ensure flux through the membrane did not change over time. Pure water flux results at both operating pressures are shown in S-7. After compaction occurred, the suspension was fed through the membrane at a pressure of either 1 or 2 bar. PTFE tubing was used for all connections to minimize particle adhesion and loss. All experiments were performed in triplicate.

The permeate suspension was collected via a flask with a minimal opening to decrease contamination by air particles. The flask was placed on a Mettler Toledo balance where the flux through the membranes was found by mass collected over a 5 s time period. Metter Toledo Balance Link software was utilized for saving these data from the balance. The flux (*J*) of the suspension through the membrane was determined using the following equation:

$$J = \frac{\text{Volume}}{\text{Area} \cdot \text{Time}}$$

Nanoparticle concentrations were determined in triplicate by utilizing fluorescent intensity measurements with a 96-well black clear-bottom well plate placed in a BioTeck Synergy hybrid microplate reader. All suspensions were diluted to one-part nanoparticle suspension to three-part water and evaluated in triplicate to ensure accurate readings. The experimental setup is outlined in S-8.

#### 3. RESULTS

**3.1. Microfiltration Membrane Characterization.** Four different membranes were chosen to test the impact of different membrane characteristics, including pore structure, porosity, hydrophilicity, and thickness, on viral vector purification. The properties of each membrane used in this study are highlighted in Table 1. PC-Lazer-Sym is a symmetric

ACS Applied Bio Materials www.acsabm.org Article

Table 1. Microfiltration Membrane's Characteristics

Properties	PC-Lazer-Sym	PVDF-Sponge-Sym	PVDF-Sponge-Asym	PES-Sponge-Asym
Polymer type <sup>a</sup>	Polycarbonate	Polyvinylidene fluoride	Polyvinylidene fluoride	Polyethersulfone
Pore size (nm) <sup>a</sup>	200	220	$45-200^{42}$	220
Thickness $(\mu m)^b$	25	125	165	165
Volumetric porosity (%) <sup>b</sup>	$33.66 \pm 3$	$65.39 \pm 5$	$64.49 \pm 4$	$85.65 \pm 7$
Contact angle (deg) <sup>c</sup>	$64.1 \pm 0.9$	$56.4 \pm 0.54$	$57.8 \pm 5.6$	$41.1 \pm 8.2$
Zeta potential (mV) <sup>d</sup>	$-15-25^{43}$	$-15-20^{44}$	$-15^{45}$	$-15-20^{46,47}$
Pore structure	Laser etched-symmetric	Spongelike-symmetric	Spongelike-asymmetric	Spongelike—asymmetric

"Provided by manufacturer (MilliporeSigma); PVDF-Sponge-Asym found in literature. <sup>b</sup>Determined utilizing gas pycnometer. <sup>c</sup>Initial contact angle documented. Contact angle over time is highlighted in Figure S-5. <sup>d</sup>Zeta Potential at a pH of 7 found in literature.

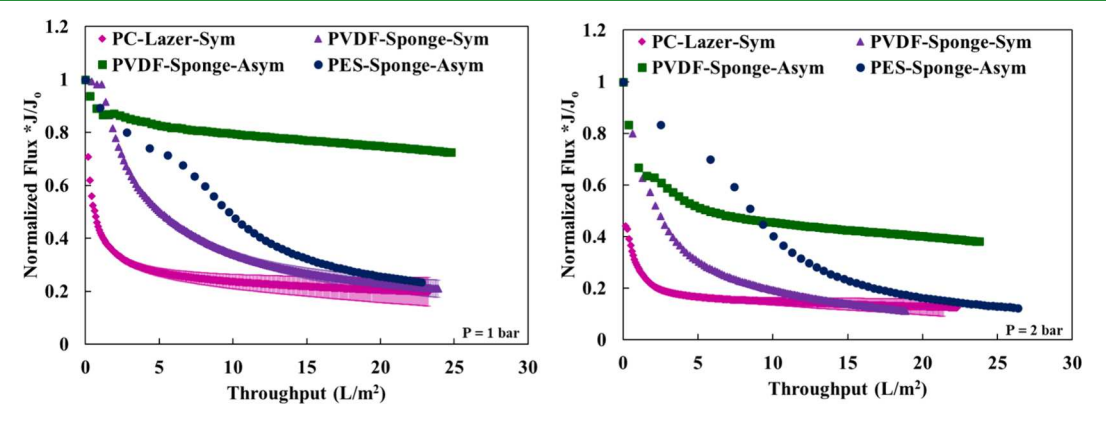
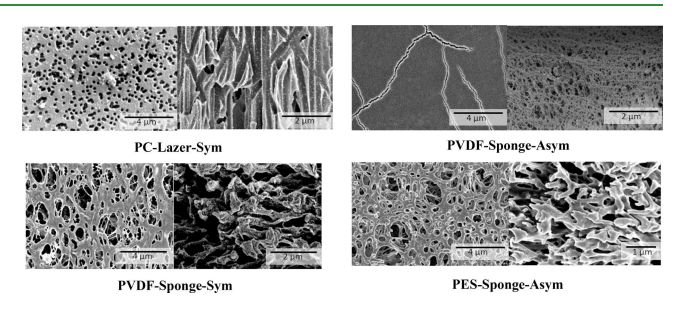


Figure 1. Model viral vector only (10<sup>14</sup> particles/mL in Type I/II water) normalized flux as a function of volumetric throughput for the four membranes tested at an operational pressure of 1 bar (left) and 2 bar (right). Error bars represent the standard deviation of 3 different measurements.

polycarbonate (PC) membrane with a hydrophilic surface with laser-etched cylindrical pores. PVDF-Sponge-Sym is a spongelike membrane with a hydrophilic surface and a similar symmetric pore density throughout the entire thickness of the membrane. PVDF-Sponge-Asym has a small pore size on the surface of the membrane and for the first 65  $\mu$ m depth of the membrane. 42 The other portion of the membrane consists of a polyester backing ( $\sim 100 \ \mu m$  thickness<sup>42</sup>) material with very open pore structure. PES-Sponge-Asym is a sponge-like membrane with a hydrophilic surface and a pore structure representing a funnel type structure. The intended flow path indicated by the supplier is to allow the solution to flow from the open pore structure into the smaller side; however, for this application, we chose to flip this membrane to have the suspension flow from the smaller pore structure to the larger open pore structure.

**3.2. Model Viral Vector Only Filtration.** The membranes discussed in Section 2.1 were challenged with 20 nm green fluorescent silica nanoparticle suspension discussed in Section 2.3.1.1 at a constant pressure of 1 and 2 bar, with the data for the normalized flux as a function of volumetric throughput shown in Figure 1. All membranes showed rapid flux decline, indicating substantial fouling. Furthermore, the flux decline was impacted by operating pressure, with the higher operating pressure flux decline being higher than the lower operating pressure, possibly indicating enhanced cake layer compaction. These results indicate that operating at lower pressures shows less significant flux decline, indicating reduced fouling.

SEM images taken after filtration experiments illustrate fouling in Figure 2. These findings indicated the pivotal role played by pore size and pore structure on the throughput and fouling behavior of model viral vectors. When comparing the



**Figure 2.** SEM images after model viral vector filtration for all four membranes. Surface images shown on left. Cross section images shown on right.

symmetric membranes with the asymmetric membranes, the symmetric membranes show significant pore entrapment of particles rather than cake layer formation on the surface. One of the asymmetric membranes (PVDF-Sponge-Asym), on the other hand, shows significant cake layer formation when compared to pristine images in S-9. These outcomes underscore the significance of pore size in the recovery of model viral vectors. Moreover, PES-Sponge-Asym exhibits the least pore entrapment both on the surface and in the pore channels, a characteristic corroborated by the remarkable recovery rate (~100% at 1 bar). This recovery is higher than the typical centrifugation recovery rate (~70–90%). S,37,48–50

Table 2 summarizes the model viral vector recovery and the operating time of the four membranes. The recovery was determined as the ratio of suspension fluorescent intensity in the permeate samples to that in the feed:

Table 2. Model Viral Vector Filtration Recovery and Operating Time for a Throughput of 20  $L/m^2$  at Two Operating Pressures<sup>a</sup>

		PC-Lazer-Sym	PVDF-Sponge-Sym	PVDF-Sponge-Asym	PES-Sponge-Asym
1 bar	Recovery (%)	$71.6 \pm 5.1$	$85.0 \pm 3.6$	$69.1 \pm 1.3$	$104.2 \pm 6.8$
	Operating time (h)	$0.6 \pm 0.05$	$0.3 \pm 0.04$	$0.1 \pm 0.01$	$0.1 \pm 0.07$
2 bar	Recovery (%)	$58.8 \pm 3.6$	$91.1 \pm 6.2$	$60.8 \pm 0.3$	$92.2 \pm 1.6$
	Operating time (h)	$0.6 \pm 0.04$	$0.3 \pm 0.06$	$0.1 \pm 0.30$	$0.04 \pm 0.02$

<sup>a</sup>Error represents the standard deviation of 3 different measurements.

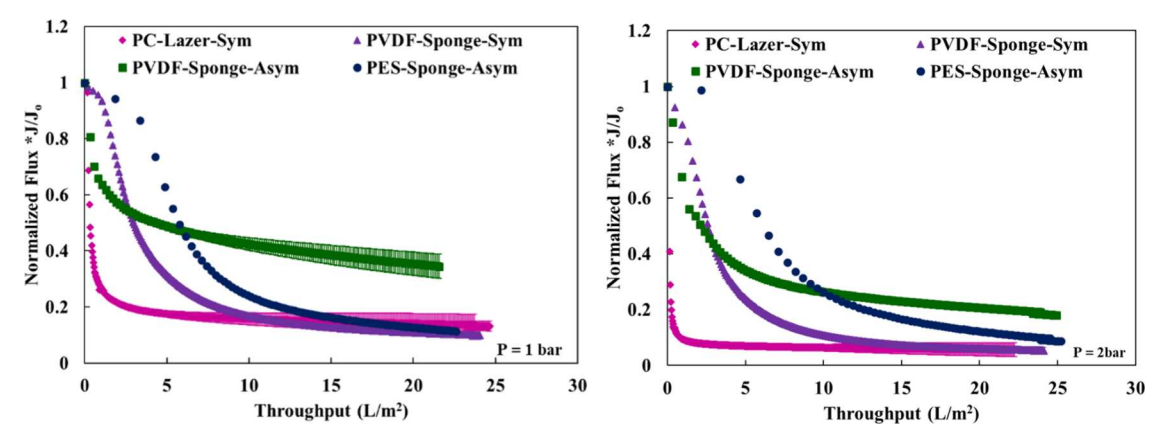


Figure 3. Model mixture normalized flux as a function of volumetric throughput for four membranes tested at operating pressures of 1 bar (left) and 2 bar (right). Error bars represent the standard deviation of 3 different measurements.

$$Recover(\%) = \frac{I_{permeate}}{I_{feed}}$$

The recovery results show that with increasing operating pressure decreases in recovery are seen, thus indicating nanoparticle exclusion or entrapment by the surface cake layer. This may be attributed to increased compaction of any formed cake layer, resulting in an increased retention of viral vectors. Moreover, PES-Sponge-Asym shows the highest recovery (~100% at 1 bar) and 100-time reduction in operating time compared to typical overnight centrifugation used for viral vector purification. 5,37,48-50

3.3. Model Viral Vector Mixture Filtration. To better understand how a realistic viral vector mixture may perform, we evaluated a mixture containing 20 nm green fluorescent silica nanoparticles, 200 nm red fluorescent silica nanoparticles, and BSA discussed in Section 2.3.1.2. The membranes discussed in Section 2.1 were challenged with the suspension at constant pressures of 1 and 2 bar. Figure 3 shows similar results that were seen with the model viral vector only filtration with a slight increase in the flux decline. For example, at an operating pressure of 1 bar, when the membranes were challenged with model viral vectors only, the flux decline was between 70% and 30% the original flux whereas when challenged with the mixture, the flux decline was between 35% and 10% of the original flux. The operating pressure's negative impact on the filtration behavior indicated the need to operate at low pressures. The normalized flux as a function of volumetric throughput indicated significant fouling behavior shown by the flux decline.

SEM images illustrate the fouling dynamics observed post mixture filtration, shown in Figure 4. As in the prior case, the asymmetric membranes exhibited cake layer formation and minimal pore entrapment behavior. The symmetric membranes, however, exhibited minimal cake layer formation, and

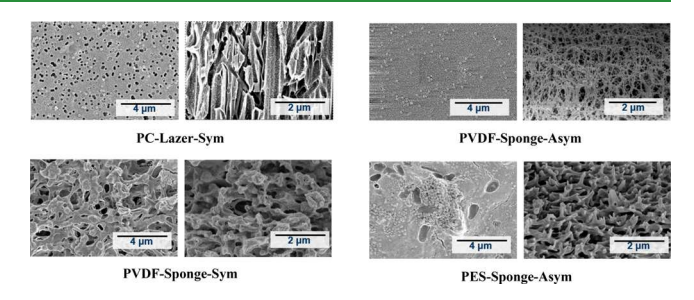


Figure 4. SEM of surface (left) and cross section (right) after model mixture filtration for four membranes tested.

most fouling behavior is exhibited by pore entrapment of the particles.

Recovery and operating results were slightly decreased by the complexity of the mixture, as shown in Table 3. PES-Sponge-Asym still exhibited the highest recovery ( $\sim$ 85%) with the lowest operating time.

**3.4. Buffer Effects.** Viral vector synthesis uses cell media, which includes buffers and salts. To assess the impact of these components, we added Tris buffer plus saline (150 mM NaCl) to our model viral vector mixture filtration. We focused our attention particularly on PES-Sponge-Asym, which exhibited the lowest operating time and the highest product recovery. Our investigation revealed a significant decline in flux when Tris buffer was employed, seen in Figure 5. This phenomenon could be attributed, in part, to the observed increase in the hydrodynamic diameter of BSA in the presence of Tris buffer, as corroborated by our dynamic light scattering (DLS) results shown in Figure 5. These observations are in agreement with the research conducted by Taha and Lee where the effect of Tris buffer on the hydrodynamic diameter of BSA was assessed.<sup>51</sup> Their study established a clear connection between higher buffer concentrations and the hydrodynamic diameter of BSA, which, in turn, may be the driving force behind the

Table 3. Model Mixture Filtration Recovery, Purity, and Operating Time for a throughput of 20  $L/m^2$  at Two Operating Pressures<sup>a</sup>

		PC-Lazer-Sym	PVDF-Sponge-Sym	PVDF-Sponge-Asym	PES-Sponge-Asym
1 bar	Recovery (%)	$76.2 \pm 9.0$	$68.3 \pm 7.2$	$73.1 \pm 2.8$	$85.3 \pm 1.7$
	Operating time (h)	$1.6 \pm 0.10$	$1.2 \pm 0.10$	$0.3 \pm 0.05$	$0.2 \pm 0.04$
	Purity (%)	$79.7 \pm 2.5$	$81.4 \pm 3.5$	$80.3 \pm 1.8$	$82.7 \pm 1.8$
2 bar	Recovery (%)	$60.1 \pm 11.0$	$75.8 \pm 5.5$	$57.6 \pm 5.4$	$83.6 \pm 3.3$
	Operating time (h)	$1.8 \pm 0.10$	$1.2 \pm 0.10$	$0.2 \pm 0.01$	$0.1 \pm 0.01$
	Purity (%)	$75.5 \pm 3.0$	$79.3 \pm 4.3$	$76.1 \pm 2.0$	$83.2 \pm 1.5$

<sup>&</sup>lt;sup>a</sup>Error represents the standard deviation of three different measurements.

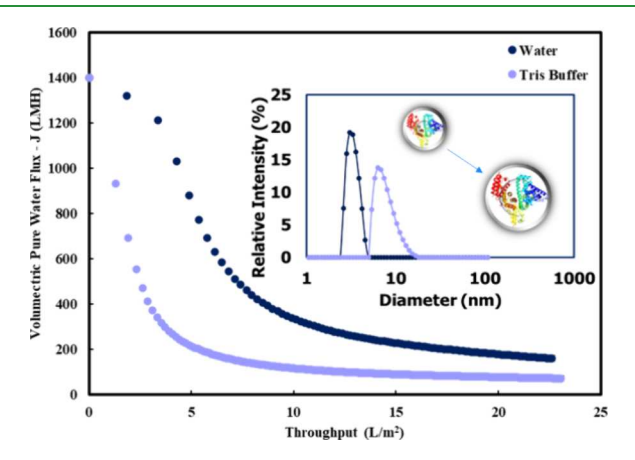


**Figure 5.** Tris buffer plus saline solution (150 mM NaCl) effect on PES-Sponge-Asym model mixture filtration showed an increase in flux decline, indicating more fouling behavior. DLS results shown an increase in diameter of BSA.

more pronounced fouling behavior evident in our declining flux results. Moreover, this buffer-related impact on filtration mirrors the findings of Chu et al., who, while investigating a similar system involving viral vector-like nanoparticles, observed an elevation in transmembrane pressure with increasing buffer concentration. This observation suggests heightened fouling behavior with increasing buffer concentrations. Our research underscores the critical role of buffer composition in membrane-based viral vector purification, given its substantial impact on filtration performance.

**3.5. Fouling Models.** We adopted a comprehensive approach to evaluate our experimental findings by utilizing well-established fouling models, specifically the complete blocking, standard blocking, intermediate blocking, and cake layer models, shown in Table 4. <sup>10,39,41</sup>

Table 4. Fouling Models for Constant Pressure Filtration<sup>a</sup>

Complete blocking	Standard blocking	Intermediate blocking	Cake layer
$ \ln J = \ln J_{o} - K_{B}t $	$\sqrt{J} = \sqrt{J_{\rm o}} - \frac{K_{\rm S}\sqrt{J_{\rm o}}}{2}v$	$ \ln J = \ln J_{o} - K_{I}\nu $	$\frac{t}{v} = \frac{1}{J_o} + K_C v$

 $^aJ_{\rm o}$  is the initial flux,  $K_{\rm B}$ ,  $K_{\rm S}$ ,  $K_{\rm D}$  and  $K_{\rm c}$  are the fouling constants,  $\nu$  is the throughput, and t is the time.

These models are instrumental in offering theoretical insights into the dynamics of fouling, contributing to our understanding of control and prevention strategies. The complete blocking model posits that particles entirely block the membrane pores, impeding fluid flow. The standard blocking model, on the other hand, assumes that fouling occurs

within the membrane pores, leading to a gradual reduction in the pore diameter. Intermediate blocking incorporates aspects of both complete and standard blocking, considering scenarios where particles partially block pores. In the cake layer model, it is assumed that particles in the feed solution accumulate on the membrane surface, forming a cake-like layer. This model considers the resistance posed by the cake layer, which is characterized by its thickness and porosity. These models incorporate the concept of a resistance-in-series model, where the total resistance to filtration is divided into different components, such as cake layer resistance or external or internal pore blocking. These models are valuable for understanding fouling dynamics and guiding membrane design. However, they necessitate certain assumptions, including the uniformity of the particle size, steady-state conditions, and simplified pore structures. Limitations arise from oversimplifications, as real-world fouling is often influenced by complex interactions, variations in particle size distributions, and dynamic operating conditions.

In our investigation, we observed that during model mixture filtration, asymmetric membranes exhibited distinct characteristics. SEM imaging revealed clear evidence of cake layer formation, which was further corroborated by the excellent fit with the cake layer model, yielding an  $R^2$  value exceeding 0.98 shown Figure 6d. This observation implies that the accumulation of particles on the membrane surface resembled the formation of a cake-like layer, indicating a specific fouling behavior associated with this membrane pore structure.

Conversely, for PC-Lazer-Sym, which features an isoporous symmetric design, SEM imaging pointed to the external and internal pore entrapment of particles. This observation aligned with the outcomes predicted by the complete, intermediate, and standard blocking models (Figure 6a-c) The prevalence of pore entrapment suggests a different fouling mechanism (such as, inertial impaction leading to particle adhesion in pores), distinct from the cake layer formation observed in asymmetric membranes.

Our utilization of fouling models has provided the needed quantifications into the distinct fouling behaviors exhibited by asymmetric and symmetric membranes. These findings not only enhance our understanding of fouling dynamics but also guide the development of strategies to mitigate fouling in membrane-based viral vector purification processes.

**3.6.** Principal Component Analysis (PCA) and Trends. Principal Component Analysis (PCA) is a powerful statistical technique used to reduce the dimensionality of complex data sets, enabling us to uncover meaningful patterns and relationships among variables. PCA works by transforming the original variables into a new set of uncorrelated variables called principal components. These principal components are linear combinations of the original variables and are ordered in

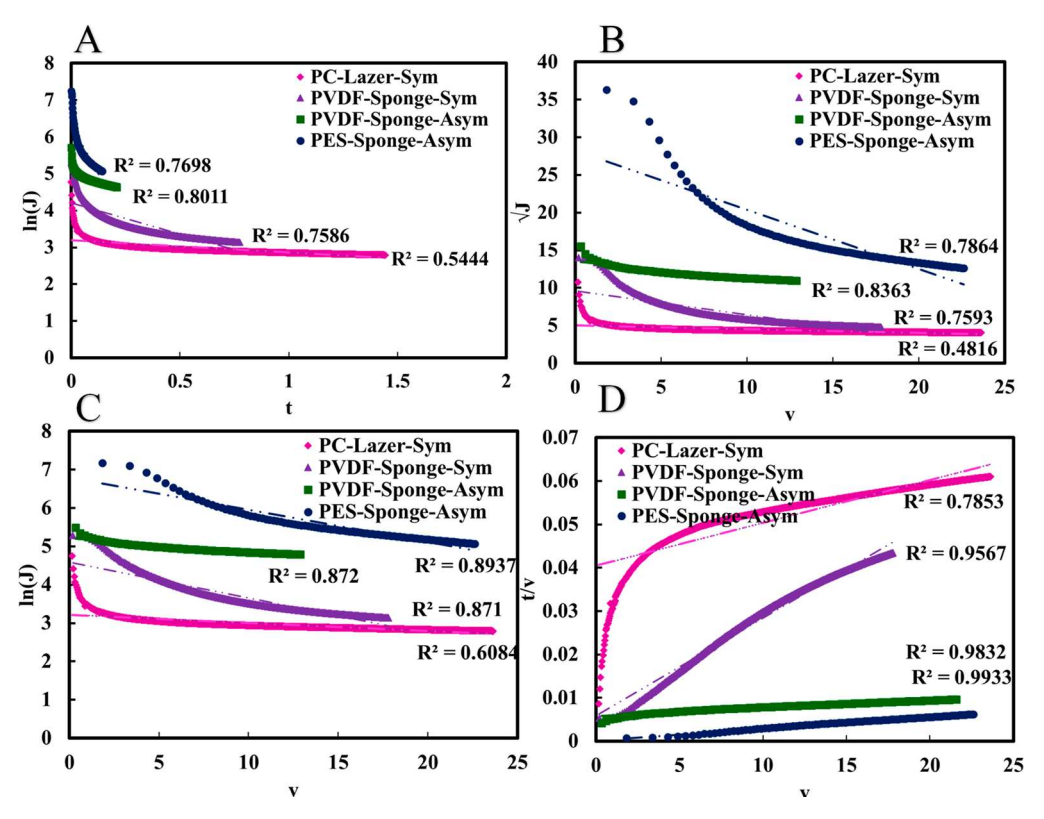
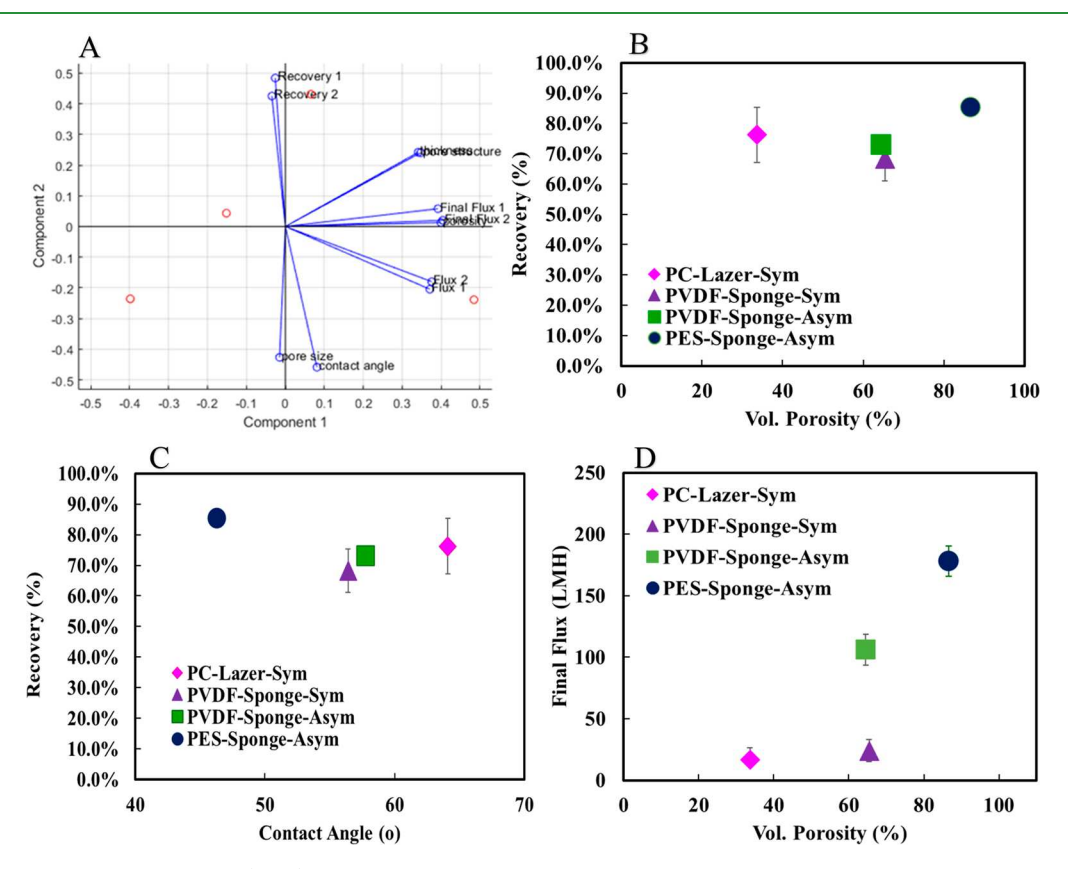


Figure 6. Fouling models for experimental model mixture results at an operating pressure of 1 bar. (A) Complete blocking model; (B) standard blocking model; (C) intermediate blocking model; and (D) cake layer.



**Figure 7.** Principal component analysis (PCA) in Graph A elucidates crucial trends in membrane properties impacting viral vector recovery. Subsequent graphs further delineate the key relationships: Graph B illustrates the positive correlation between porosity and recovery; Graph C depicts the impact of hydrophilicity (shown via contact angle) on recovery, and Graph D showcases the relationship between porosity and final flux of different pore structures. Error bars represent the standard deviation of 3 different measurements.

terms of the variance they capture with the first component explaining the most variance in the data.

In the context of our research on membrane properties and their impact on recovery and operating time in viral vector purification, PCA serves as a valuable tool for several reasons. First, it allows us to condense the information from multiple variables into a smaller set of components, simplifying the interpretation of data. This is particularly useful when dealing with a large number of membrane characteristics as it reduces the complexity of the analysis. Second, PCA helps identify which variables are most influential in driving the observed trends in recovery and operating time. By examining the loadings of each variable on the principal components, we can determine the strength and direction of their relationships with the outcomes of interest.

Our results from PCA for our model viral vector throughput are shown in Figure 7a. Our principal components were mostly attributed to the final steady state flux seen through the membrane and the recovery of the model viral vectors. As expected, porosity displayed a positive correlation with the final flux, indicating that membranes with higher porosity tend to have better throughput, potentially reducing the operating time. Furthermore, more hydrophilic membranes, as indicated by a lower contact angle, are associated with higher recovery rates. Pore structure and thickness displayed a slightly positive correlation with both final flux and recovery, indicating their potential role in enhancing these outcomes.

These findings are invaluable in guiding the selection and design of membranes for viral vector purification processes as they highlight specific membrane properties that can be optimized to achieve desired recovery and operating time goals. By utilizing PCA, we are able to distill complex data into actionable insights, improving the efficiency and effectiveness of our bioprocessing techniques.

## 4. CONCLUSION

This research has advanced our understanding of membrane-based strategies for the purification of viral vectors, addressing the highly important aspects of the particle recovery efficiency and operating time. The importance of viral vector purification in gene therapy and biotechnology cannot be overstated, and our systematic investigation of membrane properties has provided key insights that contribute to the optimization of this critical bioprocessing step.

The distinction in fouling behaviors between symmetric and asymmetric membranes sheds light on the dynamics of membrane-particle interactions. Understanding that symmetric membranes tend to foul within the pores, while asymmetric membranes form a cake layer on the surface guides future membrane selection based on the specific fouling challenges encountered in viral vector purification processes. Moreover, the positive correlation between hydrophilicity and recovery underscores the significance of surface properties in enhancing recovery. This finding informs membrane modification strategies, emphasizing the potential of increasing the hydrophilicity for improved recovery. The relationship between porosity and various outcomes, including throughput, operating time, and recovery, provides a comprehensive understanding of how this parameter influences the overall process performance. Membranes with higher porosity demonstrated superior outcomes across these metrics, highlighting the critical role of porosity in optimizing viral vector purification. Notably, the asymmetric PES membrane emerged as the

optimal choice, achieving remarkable recovery rates, substantial reductions in the model cell debris and BSA, and the fastest operating time. These types of hydrophilized membranes and porosities are good choices for future viral vector purification processes, contributing to the advancement of gene therapy and biotechnology.

This research not only fills gaps in our current understanding of membrane characteristics during viral vector purification but also offers tangible insights that can be applied to enhance the efficiency, specificity, and quality of viral vector production. It is crucial to acknowledge that our study utilizes model systems with AAV-sized nanoparticles and that real-world applications may present additional complexities. Future investigations involving authentic viral vectors are necessary to validate and refine our findings. Nevertheless, our results offer a valuable starting point for membrane selection in practical applications, providing insights into the impact of key membrane properties on the viral vector recovery. The outcomes presented can pave the way for further innovations in membrane-based bioprocessing, fostering progress in the broader field of gene therapy and biotechnology.

### ASSOCIATED CONTENT

# **5** Supporting Information

The Supporting Information is available free of charge at https://pubs.acs.org/doi/10.1021/acsabm.4c00272.

Additional experimental details, materials, and methods, including SEM images and a photograph of the experimental setup (PDF)

# AUTHOR INFORMATION

# **Corresponding Authors**

Dibakar Bhattacharyya — Department of Chemical and Materials Engineering, University of Kentucky, Lexington, Kentucky 40506, United States; orcid.org/0000-0001-9948-9085; Email: db@uky.edu

Malgorzata Chwatko – Department of Chemical and Materials Engineering, University of Kentucky, Lexington, Kentucky 40506, United States; orcid.org/0000-0002-2770-5196; Email: m.chwatko@uky.edu

### Authors

Mara Leach – Department of Chemical and Materials
Engineering, University of Kentucky, Lexington, Kentucky
40506, United States; orcid.org/0009-0005-5655-7646

Catherine Cox – Department of Chemical and Materials Engineering, University of Kentucky, Lexington, Kentucky 40506, United States

Sumith Ranil Wickramasinghe — Department of Chemical Engineering, University of Arkansas, Fayetteville, Arkansas 72701, United States

Complete contact information is available at: https://pubs.acs.org/10.1021/acsabm.4c00272

# **Author Contributions**

Mara Leach conducted all experiments, carried out data analysis, and contributed significantly to the writing of the manuscript. Catherine Cox actively participated in experimental work. Ranil Wickramasinghe contributed to manuscript review. Malgorzata Chwatko and Dibakar Bhattacharyya supervised the study, provided guidance throughout the research process, and played integral roles in reviewing and

contributing to the manuscript. All authors have read and approved the final version of the manuscript.

#### **Funding**

This work was supported through the University of Kentucky Pigman College of Chemical and Materials Engineering and is funded by grant number 2218054 from the NSF EPSCoR grant.

#### **Notes**

The authors declare no competing financial interest.

## ACKNOWLEDGMENTS

The authors acknowledge the NSF EPSCoR grant 2218054. The authors also acknowledge Solecta Membranes (Oceanside, CA) for providing large-sheet commercial PVDF400 membranes and Nico Briot at the Electron Microscopy Center (University of Kentucky) for SEM/EDX instrumentation.

## REFERENCES

- (1) Srivastava, A.; Mallela, K. M. G.; Deorkar, N.; Brophy, G. Manufacturing Challenges and Rational Formulation Development for AAV Viral Vectors. *J. Pharm. Sci.* **2021**, *110* (7), 2609–2624.
- (2) Grieger, J. C.; Choi, V. W.; Samulski, R. J. Production and characterization of adeno-associated viral vectors. *Nat. Protoc.* **2006**, *1* (3), 1412–1428.
- (3) Singh, N.; Heldt, C. L. Challenges in downstream purification of gene therapy viral vectors. *Current Opinion in Chemical Engineering* **2022**, 35, 100780.
- (4) Besnard, L.; Fabre, V.; Fettig, M.; Gousseinov, E.; Kawakami, Y.; Laroudie, N.; Scanlan, C.; Pattnaik, P. Clarification of vaccines: An overview of filter based technology trends and best practices. *Biotechnol. Adv.* **2016**, *34* (1), 1–13.
- (5) Hermens, W.; Ter Brake, O.; Dijkhuizen, P. A.; Sonnemans, M. A. F.; Grimm, D.; Kleinschmidt, J. A.; Verhaagen, J. Purification of recombinant adeno-associated virus by iodixanol gradient ultracentrifugation allows rapid and reproducible preparation of vector stocks for gene transfer in the nervous system. *Hum. Gene Ther.* 1999, 10 (11), 1885–1891.
- (6) Mcintosh, N. L.; Berguig, G. Y.; Karim, O. A.; Cortesio, C. L.; De Angelis, R.; Khan, A. A.; Gold, D.; Maga, J. A.; Bhat, V. S. Comprehensive characterization and quantification of adeno associated vectors by size exclusion chromatography and multi angle light scattering. *Sci. Rep.* **2021**, *11* (1), DOI: 10.1038/s41598-021-82599-1.
- (7) Hadpe, S. R.; Mohite, V.; Alva, S.; Rathore, A. S. Pretreatments for enhancing clarification efficiency of depth filtration during production of monoclonal antibody therapeutics. *Biotechnol. Prog.* **2020**, *36* (5), 13.
- (8) van Reis, R.; Zydney, A. Membrane separations in biotechnology. Curr. Opin. Biotechnol. 2001, 12 (2), 208–211.
- (9) Tomic, S.; Besnard, L.; Fürst, B.; Reithmeier, R.; Wichmann, R.; Schelling, P.; Hakemeyer, C. Complete clarification solution for processing high density cell culture harvests. *Sep. Purif. Technol.* **2015**, 141, 269–275.
- (10) Iritani, E.; Katagiri, N. Developments of Blocking Filtration Model in Membrane Filtration. *KONA Powder and Particle Journal* **2016**, 33 (0), 179–202.
- (11) Bandeira, V.; Peixoto, C.; Rodrigues, A. F.; Cruz, P. E.; Alves, P. M.; Coroadinha, A. S.; Carrondo, M. J. T. Downstream Processing of Lentiviral Vectors: Releasing Bottlenecks. *Hum. Gene Ther. Methods* **2012**, 23 (4), 255–263.
- (12) Wang, S. B.; Godfrey, S.; Radoniqi, F.; Lin, H.; Coffman, J. Larger Pore Size Hollow Fiber Membranes as a Solution to the Product Retention Issue in Filtration-Based Perfusion Bioreactors. *Biotechnol. J.* **2019**, *14* (2), 6.
- (13) Hadpe, S. R.; Sharma, A. K.; Mohite, V. V.; Rathore, A. S. ATF for cell culture harvest clarification: mechanistic modelling and

- comparison with TFF. J. Chem. Technol. Biotechnol. 2017, 92 (4), 732-740.
- (14) Nestola, P.; Peixoto, C.; Silva, R. R. J. S.; Alves, P. M.; Mota, J. P. B.; Carrondo, M. J. T. Improved virus purification processes for vaccines and gene therapy. *Biotechnol. Bioeng.* **2015**, *112* (5), 843–857
- (15) Negrete, A.; Pai, A.; Shiloach, J. Use of hollow fiber tangential flow filtration for the recovery and concentration of HIV virus-like particles produced in insect cells. *J. Virol. Methods* **2014**, *195*, 240–246.
- (16) Doria, M.; Ferrara, A.; Auricchio, A. AAV2/8 Vectors Purified from Culture Medium with a Simple and Rapid Protocol Transduce Murine Liver, Muscle, and Retina Efficiently. *Hum. Gene Ther. Methods* **2013**, 24 (6), 392–398.
- (17) Dalwadi, G.; Benson, H. A. E.; Chen, Y. Comparison of Diafiltration and Tangential Flow Filtration for Purification of Nanoparticle Suspensions. *Pharm. Res.* **2005**, 22 (12), 2152–2162.
- (18) Wang, Y.; Keller, K.; Cheng, X. Tangential Flow Microfiltration for Viral Separation and Concentration. *Micromachines* **2019**, *10* (5), 320
- (19) Grzenia, D. L.; Carlson, J. O.; Wickramasinghe, S. R. Tangential flow filtration for virus purification. *J. Membr. Sci.* **2008**, 321 (2), 373–380.
- (20) Nikolay, A.; De Grooth, J.; Genzel, Y.; Wood, J. A.; Reichl, U. Virus harvesting in perfusion culture: Choosing the right type of hollow fiber membrane. *Biotechnol. Bioeng.* **2020**, 117 (10), 3040–3052
- (21) Suh, D.; Jin, H.; Park, H.; Lee, C. H.; Cho, Y. H.; Baek, Y. Effect of protein fouling on filtrate flux and virus breakthrough behaviors during virus filtration process. *Biotechnol. Bioeng.* **2023**, *120* (7), 1891–1901.
- (22) Taylor, N.; Ma, W. J.; Kristopeit, A.; Wang, S. C.; Zydney, A. L. Retention characteristics of sterile filters-Effect of pore size and structure. *J. Membr. Sci.* **2021**, *635*, 119436.
- (23) Chaubal, A. S.; Zydney, A. L. Single-Pass Tangential Flow Filtration (SPTFF) of Nanoparticles: Achieving Sustainable Operation with Dilute Colloidal Suspensions for Gene Therapy Applications. *Membranes* **2023**, *13* (4), 433.
- (24) Pazouki, M.; Wilton, A. N.; Latulippe, D. R. An experimental study on sterile filtration of fluorescently labeled nanoparticles the importance of surfactant concentration. *Sep. Purif. Technol.* **2019**, 218, 217–226
- (25) Bolze, H.; Riewe, J.; Bunjes, H.; Dietzel, A.; Burg, T. P. Protective Filtration for Microfluidic Nanoparticle Precipitation for Pharmaceutical Applications. *Chem. Eng. Technol.* **2021**, *44* (3), 457–464
- (26) Kim, S.; Marion, M.; Jeong, B. H.; Hoek, E. M. V. Crossflow membrane filtration of interacting nanoparticle suspensions. *J. Membr. Sci.* **2006**, 284 (1–2), 361–372.
- (27) Sorci, M.; Woodcock, C. C.; Andersen, D. J.; Behzad, A. R.; Nunes, S.; Plawsky, J.; Belfort, G. Linking microstructure of membranes and performance. *J. Membr. Sci.* **2020**, *594*, 117419.
- (28) Chu, L.-K.; Wickramasinghe, S. R.; Qian, X.; Zydney, A. L. Retention and Fouling during Nanoparticle Filtration: Implications for Membrane Purification of Biotherapeutics. *Membranes* **2022**, *12* (3), 299.
- (29) Le Hir, M.; Wyart, Y.; Georges, G.; Siozade Lamoine, L.; Sauvade, P.; Moulin, P. Effect of salinity and nanoparticle polydispersity on UF membrane retention fouling. *J. Membr. Sci.* **2018**, 563, 405–418.
- (30) Jassby, D.; Chae, S.-R.; Hendren, Z.; Wiesner, M. Membrane filtration of fullerene nanoparticle suspensions: Effects of derivatization, pressure, electrolyte species and concentration. *J. Colloid Interface Sci.* **2010**, 346 (2), 296–302.
- (31) Kosiol, P.; Muller, M. T.; Schneider, B.; Hansmann, B.; Thom, V.; Ulbricht, M. Determination of pore size gradients of virus filtration membranes using gold nanoparticles and their relation to fouling with protein containing feed streams. *J. Membr. Sci.* **2018**, *548*, 598–608.

- (32) Hadidi, M.; Buckley, J. J.; Zydney, A. L. Ultrafiltration behavior of bacterial polysaccharides used in vaccines. *J. Membr. Sci.* **2015**, 490, 294–300.
- (33) Vicente, T.; Burri, S.; Wellnitz, S.; Walsh, K.; Rothe, S.; Liderfelt, J. Fully aseptic single-use cross flow filtration system for clarification and concentration of cytomegalovirus-like particles. *Engineering in Life Sciences* **2014**, *14* (3), 318–326.
- (34) Nestola, P.; Martins, D. L.; Peixoto, C.; Roederstein, S.; Schleuss, T.; Alves, P. M.; Mota, J. P. B.; Carrondo, M. J. T. Evaluation of Novel Large Cut-Off Ultrafiltration Membranes for Adenovirus Serotype 5 (Ad5) Concentration. *PLoS One* **2014**, *9* (12), e115802.
- (35) Hwang, K. J.; Chiang, Y. C. Comparisons of membrane fouling and separation efficiency in protein/polysaccharide cross-flow microfiltration using membranes with different morphologies. *Sep. Purif. Technol.* **2014**, *125*, 74–82.
- (36) Affandy, A.; Keshavarz-Moore, E.; Versteeg, H. K. Application of filtration blocking models to describe fouling and transmission of large plasmids DNA in sterile filtration. *J. Membr. Sci.* **2013**, 437, 150–159.
- (37) Segura, M. M.; Kamen, A. A.; Garnier, A. Overview of Current Scalable Methods for Purification of Viral Vectors. In *Viral Vectors for Gene Therapy*; Methods in Molecular Biology; Humana Press, 2011; pp 89–116.
- (38) Peixoto, C.; Ferreira, T. B.; Sousa, M. F. Q.; Carrondo, M. J. T.; Alves, P. M. Towards purification of adenoviral vectors based on membrane technology. *Biotechnol. Prog.* **2008**, 24 (6), 1290–1296.
- (39) Bolton, G.; LaCasse, D.; Kuriyel, R. Combined models of membrane fouling: Development and application to microfiltration and ultrafiltration of biological fluids. *J. Membr. Sci.* **2006**, 277 (1–2), 75–84.
- (40) Morenweiser, R. Downstream processing of viral vectors and vaccines. *Gene Ther.* **2005**, *12* (S1), S103-S110.
- (41) Huang, B.; Gu, H.; Xiao, K.; Qu, F.; Yu, H.; Wei, C. Fouling Mechanisms Analysis via Combined Fouling Models for Surface Water Ultrafiltration Process. *Membranes* **2020**, *10* (7), 149.
- (42) Mills, R.; Vogler, R. J.; Bernard, M.; Concolino, J.; Hersh, L. B.; Wei, Y. A.; Hastings, J. T.; Dziubla, T.; Baldridge, K. C.; Bhattacharyya, D. Aerosol capture and coronavirus spike protein deactivation by enzyme functionalized antiviral membranes. *Communications Materials* **2022**, *3* (1), 34.
- (43) Min, K. J.; Shul, Y. G.; Kim, H. G.; Chun, M. S.Change of surface property and flux of polycarbonate membrane by surface modification with fluorine. In *Frontiers on Separation Science and Technology*; World Scientific, 2004; pp 555–560.
- (44) Szymczyk, A.; Fievet, P.; Foissy, A. Electrokinetic characterization of porous plugs from streaming potential coupled with electrical resistance measurements. *J. Colloid Interface Sci.* **2002**, 255 (2), 323–331.
- (45) Hernández, S.; Porter, C.; Zhang, X.; Wei, Y.; Bhattacharyya, D. Layer-by-layer assembled membranes with immobilized porins. *RSC Adv.* **2017**, *7* (88), 56123–56136.
- (46) Gasch, J.; Leopold, C. S.; Knoth, H. Drug retention by inline filters Effect of positively charged polyethersulfone filter membranes on drug solutions with low concentration. *European Journal of Pharmaceutical Sciences* **2011**, *44* (1–2), 49–56.
- (47) Manawi, Y.; Kochkodan, V.; Mahmoudi, E.; Johnson, D. J.; Mohammad, A. W.; Atieh, M. A. Characterization and Separation Performance of a Novel Polyethersulfone Membrane Blended with Acacia Gum. *Sci. Rep.* **2017**, *7* (1), 15831.
- (48) Minh, A.; Kamen, A. A. Critical Assessment of Purification and Analytical Technologies for Enveloped Viral Vector and Vaccine Processing and Their Current Limitations in Resolving Co-Expressed Extracellular Vesicles. *Vaccines* **2021**, *9* (8), 823.
- (49) Duffy, A. M.; O'Doherty, A. M.; O'Brien, T.; Strappe, P. M. Purification of adenovirus and adeno-associated virus: Comparison of novel membrane-based technology to conventional techniques. *Gene Ther.* 2005, 12, S62–S72.

- (50) Moleirinho, M. G.; Silva, R. J. S.; Alves, P. M.; Carrondo, M. J. T.; Peixoto, C. Current challenges in biotherapeutic particles manufacturing. *Expert Opin. Biol. Ther.* **2020**, *20* (5), 451–465.
- (51) Taha, M.; Lee, M.-J. Interactions of TRIS [tris-(hydroxymethyl)aminomethane] and related buffers with peptide backbone: Thermodynamic characterization. *Phys. Chem. Chem. Phys.* **2010**, *12* (39), 12840.